Climate Data Record (CDR) Program

Climate Algorithm Theoretical Basis Document (C-ATBD)

ISCCP-FH Radiative Flux Profile Product

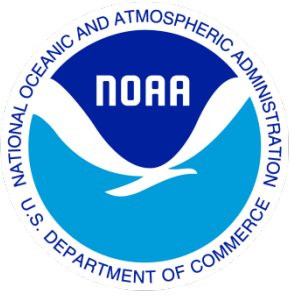

CDR Program Document Number: CDRP-ATBD-XXXX by CDRP Document Manager
Configuration Item Number: TBD from current version of CDRP-STD-0261
Revision 1.1 / <12> <18>, 2017

REVISION HISTORY

Rev.	Author	DSR No.	Description	Date
0.0	Yuanchong Zhang and William Rossow	DSR-XXX	Initial Submission to CDR Program	09/29/2014
0.1	Yuanchong Zhang	DSR-XXX	Adding cloud-caused diurnal Ta & TS adjustment	10/29/2014
0.2	Yuanchong Zhang	DSR-XXX	Adding mean TC and TB for TOA and SRF subproducts	1/30/2015
1.0	Yuanchong Zhang	DSR-XXX	Adding RS0 processing and revising H1-filling procedure TBD	7/30/2015
1.1	Yuanchong Zhang and William Rossow	DSR-XXX	Updating all for the first formal production of v.0.0 ISCCP-FH (with code v. 1.1)	12/18/2017

TABLE of CONTENTS

LIST of FIGURES

LIST of TABLES

1. Introduction

1.1 Purpose

The purpose of this document is to describe the algorithm and the data products it produces that have been submitted to the National Climatic Data Center (NCDC) by Yuanchong Zhang/Columbia University and William B. Rossow/City College of New York that will be used to create the ISCCP-FH Radiative Flux Profile Product, using the ISCCP H-series cloud climatology product that is produced based on observations of the global constellation of weather and polar-orbiting satellites and various ancillary datasets. The actual algorithm is defined by the computer program (code) that accompanies this document and thus the intent here is to provide a guide to understanding that algorithm, from both a scientific perspective and in order to assist a software engineer or end-user performing an evaluation of the code.

1.2 Definitions

Following is a summary of the symbols used to define the algorithm.

g = the cumulative probability function *(1)*

k or K = the absorption coefficient *(2)*

K = Kelven for temperature *(3)*

mb = Milli Bar = 10^{-2} Pa *(4)*

n = wavenumber *(5)*

nm = nano-meter *(6)*

μm = Micron or Micrometer *(7)*

W/m^2 or W/m^2 = Watts per square meter *(8)*

$S_{srf}\downarrow$ = Surface downward SW flux *(9)*

$S_{srf}\uparrow$ = Surface upward SW flux *(10)*

$L_{srf}\downarrow$ = Surface downward LW flux *(11)*

$L_{srf}\uparrow$ = Surface upward LW flux *(12)*

$S_{toa}\uparrow$ = TOA upward SW flux *(13)*

$L_{toa}\uparrow$ = TOA upward LW flux *(14)*

1.3 Referencing this Document

This document should be referenced as follows:

The ISCCP-FH Radiative Flux Profile Product - Climate Algorithm Theoretical Basis Document, NOAA Climate Data Record Program <CDRP-XXX-XXXX by CDRP Document Manager> Rev. 0 (2014). As NOAA CDRP was cancelled in 2015, it may still be found at http://www.ncdc.noaa.gov/cdr/operationalcdrs.html

1.4 Document Maintenance

Product Version	RadH-PRD Version	C-ATBD Version	Release Date	Notes
Test 0.0	6a	0.0	09/29/2014	
Test 0.1	6i	0.1	10/29/2014	Adding cloud-caused diurnal adjustment on TA and TS
Test 0.2	6j	0.2	1/30/2015	Adding mean TC and TB for TOA and SRF subproducts
Test 1.0	6j	1.0	7/21/2015	Adding RS0 processing and revising H1-filling procedure
0.0	a1	1.1	12/18/2017	Updating all for the first formal production

2. Observing Systems Overview

2.1 Products Generated

The ISCCP-FH Radiative Flux Profile Product generated by the algorithm described here consists of global, 110-km equal-area mapped flux components at the Top of Atmosphere (TOA), the (ocean and land) surface of the earth (SRF) and for the surface-to-TOA profile (PRF) with additional summary of or detailed information of input parameters used for the flux calculation. To meet different needs of users, it is divided into five sub-products, named (1) TOA, (2) SRF, (3) PRF, (4) MPF and (5) INP sub-products. The (1) to (3) and (5) sub-products are all at 3-hourly intervals while the (4) (MPF) is the monthly mean of the PRF sub-product. The TOA and SRF sub-products are for fluxes at TOA and surface, respectively, with supplemental summary of the most important input parameters that are used for the flux calculation. The PRF sub-product gives fluxes at 5 levels, the surface, the atmosphere at the 680, 440, 100 mb levels and TOA, with input summary parameters. The INP sub-product provides the input parameters used for the flux calculation; it may be used to reproduce ISCCP-FH product with a few additional supplementary datasets or to diagnose the physical relationship between the properties of the atmosphere and surface (including clouds and aerosols) and the radiative fluxes. The radiative fluxes include the downwelling and upwelling broadband shortwave (SW of 0.2 to 5.0 μm) and longwave (LW of 5.0 to 200 μm) fluxes, with additional downward (SW) direct and diffuse fluxes at surface, for all-sky, clear-sky and overcast conditions.

The temporal coverage is expected to be at least July 1983 to December 2015.

2.2 Instrument Characteristics

The ISCCP-FH production does not directly use instrumental observations but use the ISCCP H-series data products that are based on direct satellite observations. The ISCCP C-ATBD may be referred to for the instrumental information for better understanding of the ISCCP-FH product.

3. Algorithm Description

3.1 Algorithm Overview

The core of the algorithm is the correlated K-distribution method as described in Hansen et al. (1983) for the radiative transfer model of the NASA Goddard Institute for Space Studies (GISS) GCM Models I and II. Since then, the number of the noncontiguous correlated spectral resolution intervals, K, has been increased to obtain higher accuracy from 12 and 25 to the current 16 and 33 for SW and LW, respectively, paralleling the evolution of the GISS GCM models I and II to SI2000 (Hansen et al. 2002). The radiation part of SI2000, called RadD, was employed to produce the previous ISCCP-FD flux profile product (Zhang et al., 2004). Based on the radiation part of the current GISS GCM ModelE (Schmidt et al. 2006), called RadE, we have developed the current radiation calculation code, RadH, in which, we have added a few additional weak-SW-absorption gas species as well as the so-called flux correction factors for LW improvement, along with other new improvements implemented using the most up-to-date line-by-line results from the HITRAN2012 edition (Rothman et al., 2013). In other words, while RadH keeps the fundamental features of RadE, it is to this date the most advanced version at GISS.

The radiation code of the algorithm, RadH-PRD, is then built up on the basis of RadH. The RadH-PRD code is specifically designed to ingest ISCCP H-series products along with all other ancillary datasets to produce ISCCP-FH radiative flux profiles compiled in the five sub-products of TOA, SRF, PRF, MPF and INP as mentioned above. The whole production system using the algorithm described here is illustrated in the data flow diagram in Fig. 1 (1a and 1b).

3.2 Processing Outline

As illustrated in Fig. 1, the data flow of the whole ISCCP-FH production system is comprised of the following three stages.

Stage 1. Preprocessing.

At this stage, all necessary input parameters are extracted and preprocessed based on the original ISCCP-H datasets and some ancillary datasets. The main input data, H1, is preprocessed from HGG product (Fig. 1a) that includes all the atmospheric and surface properties as well as cloud information. The extraction results in about 130 parameters (see Appendix B for detailed description) in global, 3-hourly and 110-km equal-area mapping (1° X 1° on the equator). The 18-type cloud type information for H1 is globally incomplete so it is necessary to fill H1 to complete spatial coverage as was done for the ISCCP-FD production (Zhang et al., 2004); a similar method is used for filling H1 through a series steps by using a spatiotemporally associated H1 along with the H2 climatology, where the H2 climatology is obtained by processing ISCCP HGH and HGM (monthly mean HGG) as show in Fig. 1a. This filling procedure requires at least 3 years of data. In addition,

monthly averaged cloud fraction (CF) and amplitude of surface skin temperature (TS) and daily-mean CF are computed from H1 for cloud-caused diurnal adjustment of surface air temperature (TA), along with its near-surface air temperature (within ~100-mb from surface) and surface skin temperature (TS). The surface reflectance (RS) is determined from the original 0.65-μm aerosol-effect-corrected RS of HXG (10-km resolution) because RadH uses 0.55-μm aerosol-effect-corrected RS. All the other ancillary datasets (excluding RadH's own sets, see below), including daily snow and sea ice data and surface types etc. from ISCCP HGG and monthly aerosol data from MACv2 (improved MACv1, see Kinne et al. 2013) are also preprocessed at this stage.

Stage 2. Radiative flux calculation.

The pre-processed data sets along with other ancillary datasets, including cloud particle size climatology and Vertical Cloud Layer Configuration (VCLC) climatology, are imported into RadH-PRD to replace or reconstruct most of the model-initialization values of atmospheric and surface properties of RadH except for gas abundances. The RadH radiative transfer calculations produce the fluxes at five levels for each map grid cell every three hours for all-sky and clear-sky conditions.

Stage 3. Output.

Among the TOA, SRF, INP, PRF, INP and MPF sub-products, the first three and MPF are converted to NetCDF-4 format from the original binary format (Fig. 1b) while the fourth (INP) remains in binary format (for the reason, see Section 5.1). The detailed output information will be described in the following relevant sections.

3.3 Algorithm Input

3.3.1 Primary Sensor Data

The input datasets are the ISCCP H-series data products that are derived from weather and polar-orbit satellites sensors but the FH algorithm does not directly use primary sensor data. Since the ISCCP H-series data is treated as primary input data, Table 1 lists the data files used for this algorithm as primary input data, where ISCCP-HGG and HXG (10-km resolution) are 3-hourly while HGH and HGM are monthly-hourly and monthly, respectively. The available version at present is the v01r00 version for all ISCCP datasets.

Table 1: Primary input datasets from the ISCCP H-series

Name	Format	Version	Size	Access
ISCCP-HGG	NetCDF	v01r00	16.3 MB per file or (3-hourly) UTC	From ISCCP group
ISCCP-HGH	NetCDF	v01r00	11.3 MB per file or monthly UTC	From ISCCP group
ISCCP-HGM	NetCDF	v01r00	11.3 MB per file or month	From ISCCP group
ISCCP-HXG	NetCDF	v01r00	~40 MB per file or (3-hourly) UTC	From ISCCP group

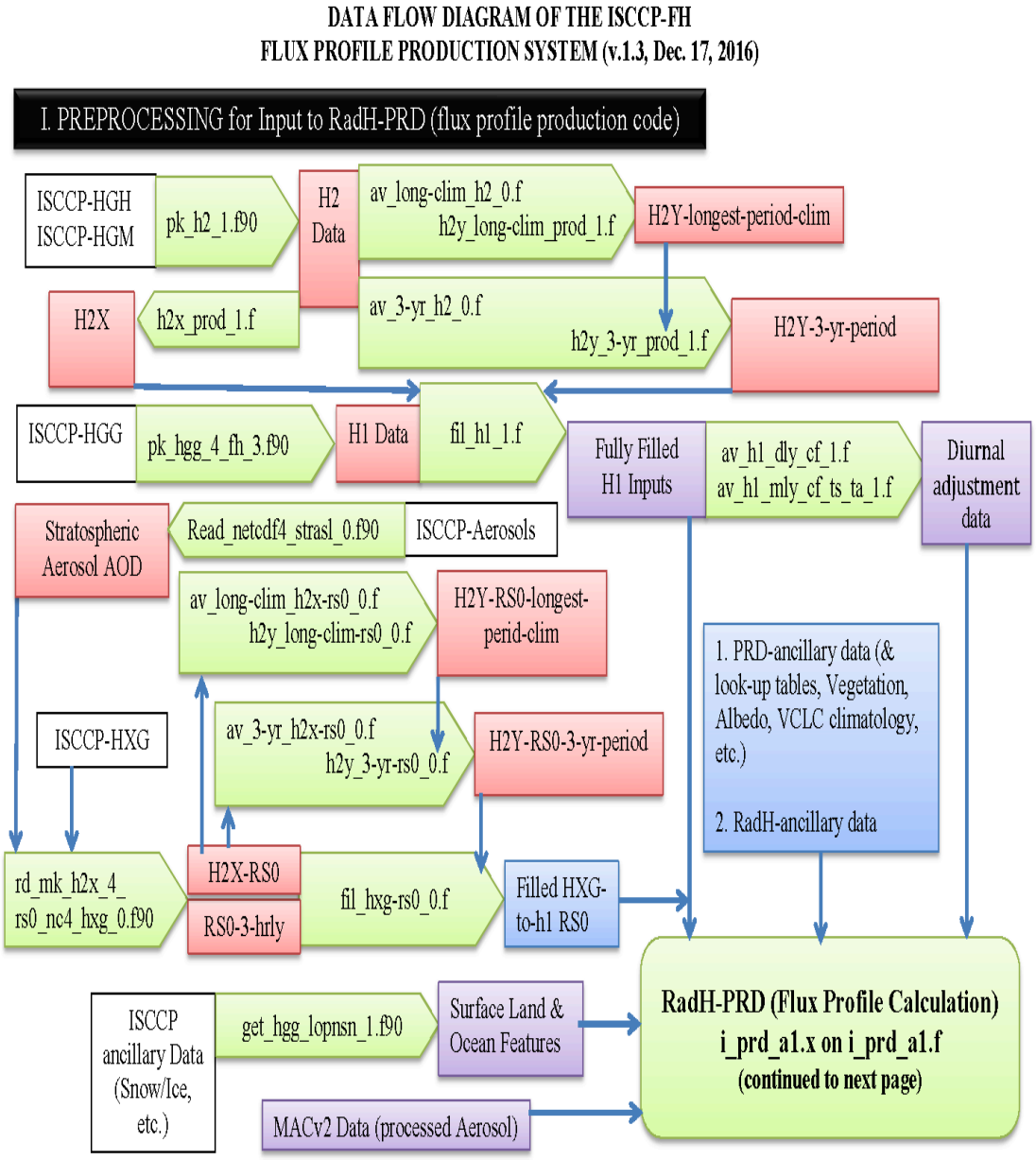

Fig. 1a: Part I of the Data flow diagram of the ISCCP-FH radiative flux production for the two stages, preprocessing and production (continued to Fig. 1b).

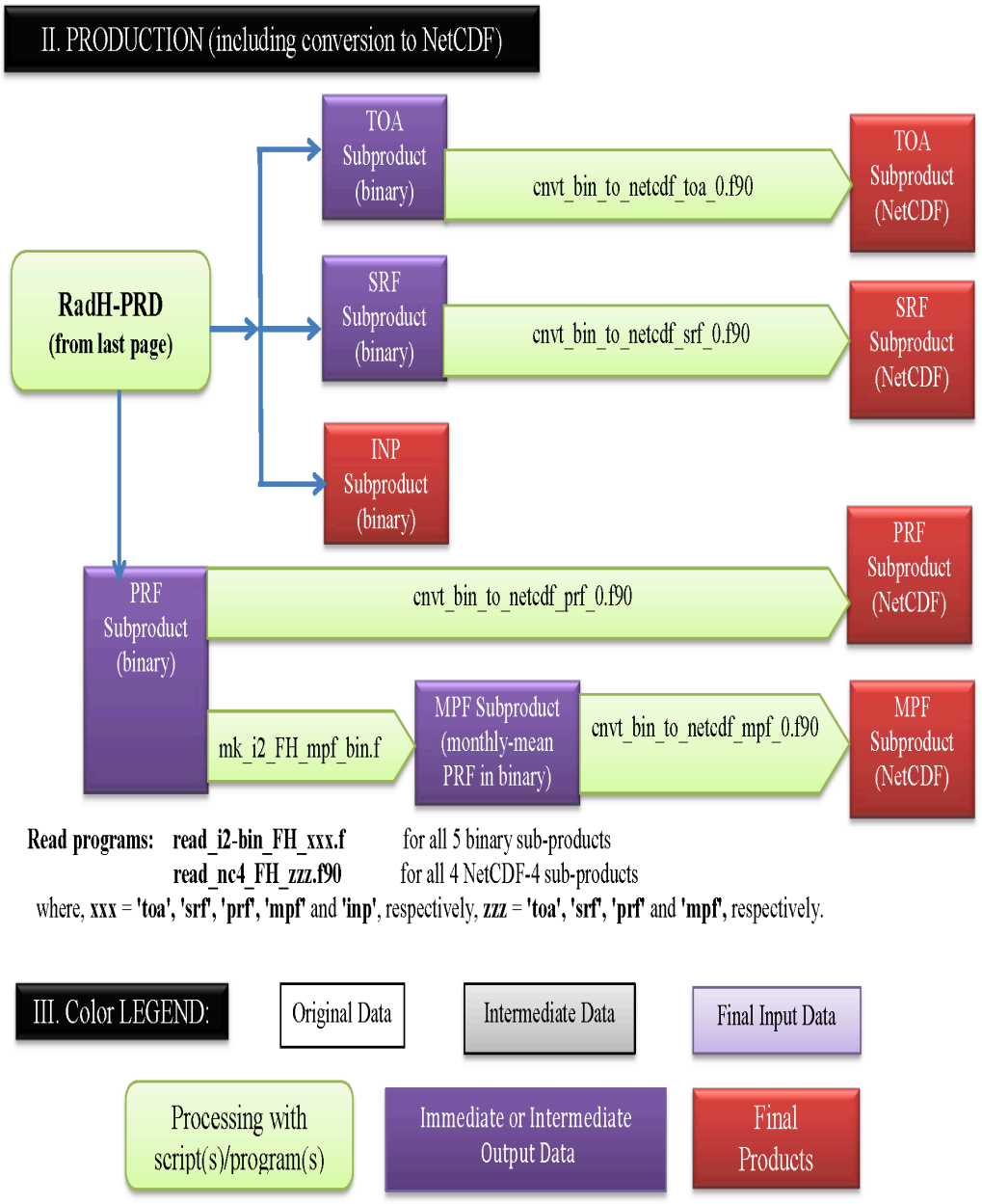

Fig. 1b: Part II of the Data flow diagram of the ISCCP-FH radiative flux production for the two stages, preprocessing and production (continued from Fig. 1a).

3.3.2 Ancillary Data

The ancillary datasets used for RadH-PRD code in this algorithm may be divided into two groups, namely, additional production-needed (PRD-ancillary data) and original RadH-initialization (RadH-ancillary data). The following Tables 2 and 3 are for so-defined PRD-ancillary and RadH-ancillary datasets, respectively.

Table 2: List of the PRD-ancillary input datasets

Name	Format	Version	Size	Access
ISCCP Surface type climatology	NetCDF	0	1.1 MB	From ISCCP group
ISCCP topography climatology	NetCDF	0	1.3	From ISCCP group
ISCCP Snow-Ice data	NetCDF	0	2.0 per day	From ISCCP group
ISCCP conversion table data from ISCCP	binary	0	2 MB / 2 files	In system
Land fraction data processed from ISCCP	binary	0	0.17 MB	In system
Land ice data processed from ISCCP	binary	0	0.17 MB	In system
1°X1° Vegetation type data	binary	0	2.7 MB	In system
110-km RS0 (reflectance from ISCCP-HXG, stratospheric aerosol-corrected only)	binary	0	0.17 MB	From processed HXG
The nnHIRS temperature and relative humidity profile datasets used by ISCCP[1]	NetCDF	0	2.6 MB in Real*4	Read from ISCCP-HGG product
GEWEX-SRB Daily TSI data for 1983 - 2013	binary	0	0.05 MB	In system
Monthly aerosol AOD, SSA and ASY	binary	MACv2	9 MB per month	Processed from original MACv2
Liquid cloud particle size climatology	binary	D0	0.04 MB	In system
Ice cloud particle size climatology	binary	D0	0.04 MB	In system
Climatology of 5-year monthly-mean surface air temperature amplitude, normalized diurnal variation, zonal-mean difference of (1) monthly-daily mean and (2) monthly-diurnal amplitude variation for Ta between 90-100% and 0-10% cloud fraction from NCEP and WWW Surface Weather station reports	binary	D0	2.9 MB/12 file	In system

[1] The 16-level Neural-Network-based HIRS temperature and humidity profile dataset is supplied by NOAA and used for ISCCP H-series production; it is directly read from the 3-hourly ISCCP-HGG product by this algorithm. Since it is actually the ancillary data used by both ISCCP H-series and ISCCP-FH production, it is also listed here for clarity.

Table 3: List of RadH-ancillary input datasets as required by original RadH

Name	Format	Version	Size	Access
1850-2050 greenhouse gases trend compilation	ASCII	E0.0	0.01 MB	In system
O3 climatology for 1850-2990 (9 files)	binary	E0.0	70 MB	In system
O3 temporal trend data	binary	E0.0	21.7 MB	In system
Koch and Bauer aerosol data climatology (9 data files)	Binary	E0.0	204 MB	In system
Monthly-mean desert dust 8-size, 9-layer AOD data	binary	E0.0	22.3 MB	In system
Monthly Volcanic AOD data	binary	E0.0	0.9 MB	In system
Monthly mean low, mid and high cloud Epsilon	binary	E0.0	0.6 MB	In system
Solar UV and solar constant variability data (1882-1998)	ASCII	E0.0	3.9 MB	In system
Vegetation type map	binary	E0.0	0.14 MB	In system
Surface water, land, sea ice and land ice map	binary	E0.0	0.12	In system

3.3.3 Derived Data

Not applicable, but there is pre-processing for non-'raw sensor' datasets as shown in Fig. 1.

3.3.4 Forward Models

See description of the radiative model in Section 3.4.1.

3.4 Theoretical Description

With all the optional parameters specified and the model initialized, the RadH-PRD code sets up from the input data the properties of the atmosphere and surface, including aerosols, gases, atmospheric vertical structure, surface features and clouds by resetting, replacing, inserting or scaling to configure the RadH's initial conditions to the desired status for the flux calculation. After the designated atmospheric constituents and properties (including clouds) and surface properties (including albedo and emissivity) are completely established, RadH-PRD calculates solar and thermal fluxes from surface to TOA, one layer by one layer, for the vertically defined atmosphere and surface, where the total vertical atmospheric layer numbers can be arbitrarily specified as needed up to 80 layers at the present (that can be changed if necessary). Such setting, resetting and calculation continues until fluxes for all cloud types (up to 18) and clear-sky scenes (defined by the mean atmospheric properties without clouds) as well as black-sky surface albedo and emissivity are produced. The code then moves to the next cell for a similar processing until

the fluxes in all the data-available grid cells (globally complete if filling is completed) are calculated for each UTC time step. The full 110-km equal-area map has 41252 cells. Then the processing proceeds to the next time UTC time and continues until each day of a month is completed, and so on.

3.4.1 Physical and Mathematical Description

The physical and mathematical basis is well described in detail in Lacis and Oinas (1991) and Liou (2002) so its mathematical and physical developments with formulas are not reproduced here. As mentioned above, the core of the algorithm is the correlated K-distribution (CKD) method. The CKD method is used to represent the spectral dependence of the radiative transfer in a vertically stratified atmosphere. The CKD method is generalized from the k-distribution (KD) method by extending it to nonhomogeneous atmospheric paths, first proposed by Lacis et al. (1979).

In the KD method, the functional space of the absorption coefficient (k) with wavenumber (n) is transformed into a cumulative probability (g) space through the intermediate k-distribution probability density function, reducing the original very-CPU-consuming line-by-line integrations in n-space to a much smaller number of sums of exponential terms in g-space with additional mathematical conveniences. This treatment greatly increases the computational efficiency without sacrificing accuracy. Because the probability density distribution of absorption coefficient strengths is derived from line-by-line calculations (in constructing either a line-by-line-based or a band-model-based k-distribution), the KD method implicitly simulates spectral integration and its precision can be increased by increasing the k-numbers to more accurately approximate the line-by-line results in more detail. The KD method also permits accurate modeling of overlapping absorption by different atmospheric gases and accurate treatment of non-gray absorption in multiply-scattering media.

However, the KD method is strictly valid only for a homogeneous atmosphere, limiting its usefulness for real atmospheres. This shortcoming is resolved by the CKD method, which assumes that the k-distributions at all altitudes are vertically correlated, though, in reality, there is some violation under some extreme situations (for a discussion of CKD validity, see Lacis and Oinas, 1991 and Liou 2002). As a result, the CKD method is a generalized method that is able to treat non-gray gaseous absorption for both solar and thermal infrared wavelengths, thermal emission, and multiple-scattering atmospheric processes associated with cloud and aerosol particles in vertically inhomogeneous atmospheres (i.e., realistic "stacked" layers with varying pressure, temperature and abundances of absorbers and scatters). The model calculates the spectral dependence of the broadband, upwelling and downwelling, SW and LW fluxes at all of the interfaces of arbitrarily specified atmospheric layers from the surface to TOA (about 100 km above mean sea level or ~ 0 mb) by summing up all the radiative transfer functions (for

transmission, multi-scattering and absorption) as functions of k for all the radiatively active media over all the k-spectral intervals.

The accuracy improvements from the earliest Models I and II to RadE and to the current RadH are through increasing the spectral representation number, K, and the accuracy of k-distribution probability density functions by using the updated line-by-line calculations with updated atmospheric constituents. The 1983 GISS radiation models I and II used 12 Ks for the SW (nominally 0.2-5.0 μ m) flux calculation and 25 Ks for the LW (nominally 5.0-200.0 μm, including one for a "window" wavelength: 11.1-11.3 μm) flux calculation (Hansen et al., 1983). The models RadD and RadE increased the k-number to 16 and 33 for SW and LW, respectively. RadD and RadE had an accuracy of 1% for cooling rates (in degree/day) throughout the troposphere and most of the stratosphere as compared with line-by-line calculations (Lacis and Oinas, 1991). Based on RadE, RadH has incorporated additional relatively weak SW-line-absorbing gases of H2O (additional lines), O2 and CO2 using the most up-to-date line-by-line results from HITRAN2012 and a refined solar calculation code that improved the atmospheric absorption for SW fluxes and virtually eliminated the bias that was found in CIRC experiment (Oreopoulos, L., et al., 2012). RadH has also improved LW calculation especially in the polar region using higher vertical resolution and better atmospheric structures. For RadH and the latest RadE, both the upward and downward fluxes agree with line-by-line fluxes to within about 1 W/m^2 for the TOA and surface LW upwelling and downwelling radiative fluxes and the SW accuracy is also close to 1% now.

Further improvements can be made in the future. The RadH-PRD has the following advantageous features: (1) The atmosphere from the surface to TOA can be physically divided into any number of layers at any pressure level so that, e.g., physical cloud layers can be positioned precisely at any altitude and interleaved with clear-air layers just like in the real world; (2) All the input parameters are physical quantities (not empirical representations) that are as realistic as possible and realistically variable in each cloud or air layer as well as at the surface. For example, each cloud layer of a multi-layer cloud system has its own top and base temperatures and pressures, optical thicknesses, and microphysical model specified by the phase, particle shape, effective particle size and size distribution variance. All air/cloud layers can also have their own aerosol mixtures with different optical properties, i.e., all the constituents and their physical properties in the model can be specified vertically independently; (3) The corresponding output fluxes are calculated for all the specified interfaces of the air/cloud layers, including TOA and the surface; (4) The model is detailed and complete (i.e., no "bulk" atmosphere, etc.) and it is physically self-consistent at all wavelengths (i.e., both SW and LW are treated using CKD method); (5) With improvements of the accuracy and knowledge of all input physical quantities, the model could be relatively easily updated to incorporate any newly available information as exemplified by the evolution of the GISS radiation code from the earliest Models I and II (Hansen et al., 1983), RadD (for ISCCP-FD, Zhang et al., 2004), RadE (Schmidt et al., 2006) to the current RadH.

For the production by this algorithm (RadH-PRD), all the gas species, including H2O, CO2, O3, O2, N2O, CH4, N2O, and chlorofluorocarbons (CFCs), and their abundances with trends and vertical/horizontal distributions are used without change (except H2O and O3, see below). The O3 vertical distribution is set by scaling the RadH vertical distribution using the ISCCP-H column O3 amount. The aerosol data from MACv2 are the central values of the column optical properties, aerosol optical depth (AOD), single scattering albedo (SSA) and size-related asymmetry-factor (ASY) for the GISS model's 6 spectral ranges (centered at 3100, 1850, 1375, 1055, 815 and, 535 nm); their vertical distribution is obtained by scaling the original RadH distribution using MACv2's column amounts and their daily values are interpolated using 3 months of data with the current month's mid-date at the center. Temperature and precipitable water are from the temperature and relative humidity of the NOAA nnHIRS data coming with ISCCP-HGG (Table 2). The land vegetation (Table 2) is from Matthews (1984) with some adjustment. The daily ISCCP snow/ice data, including land fraction and land ice climatology, are used to set surface area fractions for water, land, sea ice and land ice, with or without snow cover for land and land/ocean ice. Emissivity values for different surface types and clouds are the built-in RadH values. HXG's 10-km visible reflectance (RS) is processed and then used for the visible (VIS) albedo (0.2 to 0.7 μm) with aerosol correction; RadH's albedo ratio of near-infrared (NIR) to VIS with some adjustment based on regression with ERBE's results (Zhang et al., 2004) is used to obtain NIR albedo (0.7 to 5.0 μm). The 18 HGG cloud types (defined by phase, optical thickness and top pressure) are used to determine cloud vertical structure (CVS, Rossow et al., 2005); the vertical cloud layer configuration (VCLC) is then obtained based on CVS and cloud layer thickness climatology (as function of cloud optical thickness Tau, longitude, latitude, ocean/land, and month). The physical position of clouds is obtained using cloud top temperature (TC) by interpolating from relationship between pressure and temperature profile. The ice and liquid cloud particle size climatology from Han et al. (1994) is used to set cloud microphysical properties with ISCCP-supplied phase information. The precipitible water amount within the cloud layers is adjusted such that all the cloud layers are at 100% relative humidity.

3.4.2 Data Merging Strategy

Not applicable.

3.4.3 Numerical Strategy

The processing order of the numerical calculation is to first set up a realistic atmosphere and surface with all the specified properties and then to calculate the solar and thermal fluxes for a vertically layered grid box (location) and time. This processing continues to complete global coverage at one time step, then to all time steps.

3.4.4 Calculations

Under the work directory, on the current platforms of either Linux 3.0/3.10 or Macbook Pro OS X 10.12 platform and using Gfortran 4.8.5 version for Fortran compiler with NetCDF-4 software installed, the specific steps are listed below. Note, all the Fortran programs need specification of the year, month, dates and hours of UTC time for processing and the scripts must be customized for the user's specific directory/paths to ensure working in the particular computer environment. The version appearing in the following, e.g., '3', '1', 'a1', for the programs may be changed as necessary at the time they are submitted.

1. Preprocessing.

(Skipping climatology pre-processing that has been done and does not need to be repeated for permanent land ice, ice shelves and surface types, as well as the MACv2 aerosol data that has been processed for January 1980 to December 2040).

(1) Using script, g_ff90.z_isccp_nc4_o2.x , to compile/run pk_hgg_4_fh_3.f90 with two ISCCP utility Fortran 90 programs and some other subprogram package, etc., to extract ~130 parameters on 110-km equal-area maps from ISCCP-HGG's 3-hourly data files to get H1 data (see Fig. 1a for this and other steps below)) for the specified time in the pk_hgg_4_fh_3.f90 program.

(2) Using script, g_ff90.z_isccp_nc4_O2, to compile/run get_hgg_lopnsn_1.f90 with supplemental routine packages for preparing surface features with snow/ice information.

(3) Using pk_h2_1.f90 to pick up necessary ISCCP-HGH and HGM and processing into H2X and 3-year-H2Y.

(4) Using fil_h1_1.f to fill H1 to make it (nearly or fully) globally complete for all 18 cloud types and surface properties using H2X and H2Y.

(5) Using rd_mk_h2x_4_rs0_nc4_hxg_0.f90 to read 10-km resolution, 3-hourly HXG data and process to get non-aerosol-corrected reflectance (RS0).

(6) Compiling/run: av_h1_mly_cf_ts_ta_1.f to obtain monthly-mean cloud fraction (CF) and diurnal variation amplitude of surface skin temperature (TS).

(7) Compiling/run: av_h1_dly_cf_1.f to obtain daily-mean CF.

2. Using script, g_prd_a1.x, to link to all the RadH's original read-in ancillary data files and tables, and then compile/run i_prd_a1.f and RadH's 8-10 separated Fortran module/subprogram packages for designated time that are specified in the main Fortran (i_prd_a1.f).

3. The output sub-products are written as Integer*2 binary format as i2_toaa1.YYMMDDHH, i2_srfa1.YYMMDDHH, i2_prfa1.YYMMDDHH, and

i2_inpa1.YYMMDDHH where YY is for year (83 to 15 for 1983 to 2015), MM for month, DD for date and HH for UTC hour (00, 03, … 21) for TOA, SRF, PRF and INP sub-products. The MPF sub-product will be obtained by averaging a month of PRF sub-product. The four 3-hourly sub-products contain 19, 26, 71 and up to 335 parameter maps (of 110-km equal area) with an additional 2, 6 and 20 overcast-scene fluxes to be derived when they are used for the first 3 sub-products. MPF has the same numbers of parameters as PRF since it is just PRF's monthly average and its file name is i2_mpfa1.YYMM__...

4. Conversion of the binary to NetCDF-4 format for TOA, SRF, PRF and MPF subproducts (excluding INP subproduct, see Section 5.1 for explanation).

3.4.5 Look-Up Table Description

In the same fashion as for the above ancillary datasets, the following Tables 4 and 5 list the PRD-look-up tables and RadH-look-up tables, respectively. Note that they are all read-in tables and do not include all the numerical values explicitly defined in the original RadH's Fortran modules, subroutines and sub-functions by means of block data, data statements or simple parameter definition. These quantities are used for various specifications of standard atmospheric structures with temperature and humidity profiles for different climate zones, map grid information, background, tropospheric, stratospheric, volcanic and dust aerosols, 6-band seasonal surface albedo values for different surface features (including vegetation types and emissivity for different surface features), and for cloud characteristics, solar-zenith-angle dependence parameters for surface albedo (including sea ice and snow albedo, ocean albedo with or without foam) and wind-dependent parameters for surface emissivity, ozone absorption table, gas abundances with vertical distribution and trend, microphysical cloud model parameters, etc. It is no wonder that the above incomplete list is already so long since RadE is the radiation part of the GISS GCM that needs to calculate fluxes for various, complicated environments and conditions from surface to TOA. The details of the list of all these within-program specifications is not necessary for the C-ATBD since by selecting the condition under which one needs to calculate fluxes, RadH-PRD serves the current purpose.

Table 4: List of PRD-look-up table as input to RadH-PRD

Name	Format	Version	Size	Access
Albedo correction for partial ocean cell	binary	D0.0	0.00 MB	In system
Table for radiance and temperature conversion	binary	D0.0	0.05 MB	In system
Monthly cloud-layer thickness climatology	binary	0.0	0.1 MB	In system
Pressure-height conversion table	binary	D0.0	0.05 MB	In system
All the above were constructed by the author, Yuanchong Zhang				

Table 5: List of RadH-look-up tables as required by original RadH

Name	Format	Version	Size	Access
SW GTAU asymmetry conversion table	binary	E0.0	0.66 MB	In system
LW 33-k distribution Tau and Planck table	Binary	E0.0	3.8 MB	In system
Mie scattering parameters for aerosols and clouds	binary	E0.0	22.3 MB	In system
New LW 33-k Tau-Gas table for flux correction	binary	0.0	0.8 MB	In system
H2O continuum Tau table	binary	E0.0	0.04 MB	In system
LW top-top cloud scattering correction table	binary	E0.0	1.7 MB	In system
Near-infrared extinction table	ASCII	E0.0	0.5 MB	In system
All the above were constructed by NASA GISS radiation group with evolution from the earliest Models I and II to the current RadH.				

3.4.6 Parameterization

Not applicable.

3.4.7 Algorithm Output

The following Table 6a describes all five binary sub-products from the algorithm, where YY is for year (83 to 15 for 1983 to 2015), MM for month, DD for date and HH for UTC hour (00, 03, … 21); Table 6b for the final five subproducts for users.

Table 6a: List of the Five output sub-products (in binary) from RadH-PRD

Generic Name	File Name	Format	File Size
TOA sub-product	i2_toaa1.YYMMDDHH	binary	1.6 MB
SRF sub-product	i2_srfa1.YYMMDDHH	binary	2.25 MB
PRF sub-product	i2_prfa1.YYMMDDHH	binary	5.9 MB
INP sub-product	i2_inpa1.YYMMDDHH	binary	Up to 28 MB, but mostly < 4 MB (binary only, see text)
MPF sub-product	i2_mpfa1.YYMM__..	binary	5.9 MB

Table 6b: List of the Final Five sub-products for Version of 0.0 (code version 'a1')

Sub-product Name	File Name	Format	# of parameter	File Size
TOA	ISCCP-FH.TOA.v.0.0.GLOBAL.YYYY.MM.DD.HH.nc	NetCDF-4	23	2.9 MB
SRF	ISCCP-FH.SRF.v.0.0.GLOBAL.YYYY.MM.DD.HH.nc	NetCDF-4	34	4.5 MB
PRF	ISCCP-FH.PRF.v.0.0.GLOBAL.YYYY.MM.DD.HH.nc	NetCDF-4	91	12 MB
MPF	ISCCP-FH.MPF.v.0.0.GLOBAL.YYYY.MM.DD.HH.nc	NetCDF-4	91	12 MB
INP	i2_inpa1.YYMMDDHH, each year of which are tarred as ISCCP-FH_bin_INP_v.0.0_YYYY.tar	binary	< 335	< 28 MB

The specific output parameters and units are described in Appendix C for the TOA, SRF, PRF and INP sub-products (MPF is the same as PRF but for monthly averages).

4. Test Datasets and Outputs

4.1 Test Input Datasets

In early 2017, we have used the beta version of ISCCP-H of 2007 to test for which results were presented by Zhang et al. (2017). At the time of this writing (December, 2017), NOAA NCEI has published the first official ISCCP-H products (v01r00) for 1983 to 2009 (see www.ncdc.noaa.gov/isccp), which is used for the first, formal ISCCP-FH production (v.0.0, code version a1).

Based on this first-ever, formal production we have found the following issues, of which some may be addressed in the future version of the ISCCP-H production.

(1) Infrared cloud top temperature (IR-TC) is not filled in HGH and HGM.

(2) There exist cloud top temperature (TC) and maximum temperature of the atmospheric temperature profile (T_max) that are too high in inversion layers of atmospheric profile (most are located in polar regions, but it may be in marine stratus clouds, etc. for inversion atmospheric profile); the magnitude of them may reach > 300 K , up to 350 K. If such high temperature happens to appear, it will cause too-high precipitable water amounts (PW) in conversion to PW from relative humidity supplied by ISCCP, especially in cloud layers when the saturation is applied to them that may cause increase of PW (if the original relative humidity < 100%). At present, we simply discard those grid cells with such scenarios in the flux calculation if either (TC – T_max) > 10 K or column PW > 30 cm. The numbers of such discarded grid cells range from a few to hundreds for a global map at one UTC hour.

(3) The filling for HGG makes a global map for the H1 data (input for flux calculation) nearly complete based on 1984-2009 climatology of HGH and HGM data but there are 10 grid cells are left unfilled because they do not have any information in ISCCP-H datasets.

4.2 Test Output Analysis

4.2.1 Reproducibility

Reproducibility should be guaranteed as long as the Fortran compiler is compatible with the currently-used Gfortran 4.8.5 utilities with NetCDF-4 installed on the platforms of either Linux 3.0/3.10 or Macbook Pro OS X 10.12.

4.2.2 Precision and Accuracy

For RadH, both the upward and downward fluxes agree with line-by-line fluxes to within about 1 W/m^2. The SW accuracy is close to 1% now.

However, with RadH's good accuracy, the precision of the calculated fluxes depends on the accuracy of the input datasets. Note that the precision of the cloud and ancillary properties

from ISCCP is limited by the precision of the radiances to about 0.5%. Based on the evaluation of the ISCCP-FH products in Zhang et al. (2017), ISCCP-FH seems slightly better than ISCCP-FD, especially for atmospheric SW absorption and surface fluxes. However, the overall uncertainties essentially remain the same: $< \sim 15$ W/m^2 for TOA and $< \sim 25$ W/m^2 for Surface for regional, monthly means, but FH has higher resolution (110-km) while FD is at 250-km.

4.2.3 Error Budget

The errors and uncertainties for radiative fluxes calculated by a modern radiation model mainly come from input datasets rather than the model itself (Zhang et al., 2004). The translation of the errors or uncertainty of the input parameters into flux error estimates may be obtained by using the sensitivity test results (e.g., Zhang et al., 2006 and 2007). The following estimates are based on the sensitivity test results from Zhang et al. (1995) using radiation code of the earliest GISS GCM models II and Zhang et al. (2004, 2006 and 2007) using RadD. The values shown in Tables 7 and 8 are global averages.

Table 7: Error sources, magnitude and their caused error on Surface fluxes (in W/m^2 if there is no unit or not %)

Error sources	Error Magnitude	Error on fluxes				Perspective Improvements
		$S_{srf}\downarrow$	$S_{srf}\uparrow$	$L_{srf}\downarrow$	$L_{srf}\uparrow$	
RadH model	(see right)	1%	1%	1	1	The GISS radiation model will continue its improvements but it is no longer a major issue
temperature profile (input)	2-3 K	0.05 – 0.08	0.0	8.6 - 12.9	0.6 – 0.9	Being improved by ISCCP group
humidity profile (input)	15-25 %	0.6 - 1.1	0.06 - 0.1	4.5 - 7.5	0.2 - 0.4	Being improved by ISCCP group
Input surface reflectance	1-2 %	1.3 - 2.6	0.4 - 0.8	0.0	0.0	Being improved by ISCCP group
Input MACv2 aerosols	40 %	7,.2	1.5	0.5	0.04	No expected substantial improvement soon
Cloud amount	About 5%	6.1	1.0	4.2	0.0	Being improved by ISCCP group
Cloud Tau	10%	2.8	0.4	0.4	0.0	Being improved by ISCCP group
Cloud top Temperature	3 K	0.1	0.0	1.4	0.0	Being improved by ISCCP group

Table 8: Error sources, magnitude and the caused TOA flux error (in W/m^2 if there is no unit or not %)

Error sources	Error Magnitude	Error on fluxes		Perspective Improvements
		$S_{toa}\uparrow$	$L_{toa}\uparrow$	
RadH model	(see right)	1%	1	The GISS radiation model will continue its improvements but it is no longer a major issue
Input temperature profile	2-3 K	0.0	4.2 – 6.3	Being improved by ISCCP group
Input humidity profile	15-25 %	0.2 - 0.4	1.8 – 3.0	Being improved by ISCCP group
Input surface reflectance	1-2 %	0.8 - 1.7	0.0	Being improved by ISCCP group
Input MACv2 aerosols	40 %	2.1	0.8	No expected substantial improvement soon
Cloud amount	About 5%	5.2	2,4	Being improved by ISCCP group
Cloud Tau	10%	2.5	0.4	Being improved by ISCCP group
Cloud top Temperature	3 K	0.6	2.8	Being improved by ISCCP group

5. Practical Considerations

5.1 Numerical Computation Considerations

There is no parallelization applied in the algorithm.

The reason why the INP sub-product will not be converted to NetCDF-4 format is that, although NetCDF is able to handle the full maps of 335 parameters, the data volume grows too high: already the binary file has a size of 27 MB for one UTC hour at Integer*2 of dimension of (41252), which totals to 6.6 GB for a month (cf. ISCCP-HGG's 4 GB per month). The actual number of cloud types and layers present is usually much smaller than the defined maximum of 5-layers and 18 types, so the INP output file more typically has a size of < 4 MB for a UTC (about 1/5 of the full-mapped size). If INP sub-product saves only those maps for existing cloud layers and cloud types, which varies from grid cell to grid cell in a map, this is more economical approach and is easily handled in a binary format but is not realistically feasible in NetCDF. Moreover, the INP subproduct is expected to be used by those who intend to study it in depth and in detail so they are expected to have no difficulty using binary data format. Therefore, the INP product is not to be converted to NetCDF format that would have too-large size.

All the input and output datasets are written in Big-endian for this algorithm's operation.

5.2 Programming and Procedural Considerations

There are no apparent issues.

5.3 Quality Assessment and Diagnostics

There are several Fortran programs to read the binary sub-products and write out all the parameters in single square latitudinal and longitudinal map of (360, 180) of Real*4 maps that can be plotted by several IDL programs for review and QA. In addition, all the individual output parameters can also be replicated to square latitudinal and longitudinal map of (360,180) within RadH-PRD and written out along with the five sub-products. These replicated single-parameter maps are ready for easy IDL plotting for QA purpose. Diagnostic information for the vertical structure in a grid cell can be obtained by simply calling a subroutine. These methods may be used either for immediate QA purpose or later QA evaluations.

5.4 Exception Handling

There is no particular exception expected at the present.

5.5 Algorithm Validation

The FH version product is based on three previous analyses (Rossow and Lacis 1990, Zhang et al 1995, Zhang et al 2004), each of which was thoroughly evaluated against other flux products available at the time (Rossow and Lacis 1990, Rossow and Zhang, 1995, Zhang et al., 2006, 2007 and 2010, see also Oreopoulos et al., 2012). Substantial tests and reexamination of the new version have been executed by comparing all the twelve months of FH for 2007 based on ISCCP-H beta version in 2017 with TOA and surface observations by Zhang et al. (2017) as mentioned above. Further systematical validation of the algorithm may be performed in the same fashion as done for FD.

5.6 Processing Environment and Resources

The current ISCCP-FH production is conducted on Linux 3.0.101/x86_64 at NASA NCCS and Linux 3.10.0/x86_64 at NOAA NCEI as well as Intel core i7 Macbook Pro OS X 10.12.6 platforms using Gfortran 4.8.5 (as well as Int'l Composer XE 2013 Sp1 version on Macbook) for Fortran compilation with NetCDF-4 software installed. The CPU usage is about 8-10 hours for RadH-PRD for a month's calculation for (nearly completely) filled ISCCP-HGG at the NASA NCCS or Macbook platform but ~24 hours at the NOAA NCEI platform in addition to the pre-processing and post-flux-calculation (conversion of binary to NetCDF format) which are not substantially CPU time consuming.

The available resources at NOAA NCEI include 13 Terabytes (Tb) of storage and sufficient number of nodes as well as other supporting facilities from NASA NCCS and NASA GISS so the multi-machine operations can reduce the production time.

6. Assumptions and Limitations

There are no real assumptions and limitations for the algorithm to become operational from our experience.

6.1 Algorithm Performance

As long as the input datasets are of good quality, the algorithm is expected to perform well.

6.2 Sensor Performance

Not applicable.

7. Future Enhancements

The future enhancements concern two aspects: (1) Improvement of the input dataset quality and (2) Improvement of RadH or RadH-PRD.

7.1 Enhancement 1 – Input Data Improvement

The quality of FH depends on the quality of the input products, so there is not much to do except providing feedback to these data product producers (ISCCP, etc.). We have participated in several on-going international evaluations of these data products through WCRP/GEWEX for this purpose.

7.2 Enhancement 2 – Radiation Model Improvement

The NASA GISS radiation group continues to pursue more detail and better accuracy of the GISS radiation model.

8. References

Han, Q., W. B. Rossow, and A. A. Lacis (1994), Near-global survey of effective droplet radii in liquid water clouds using ISCCP data, J. Clim., 7, 465– 497.

Hansen, J. et al. (1983), Efficient three-dimensional global models for climate studies: Model I and II, Mon. Weather Rev., 111, 609– 662.

Kinne, S., D. O'Donnel, P. Stier, S. Kloster, K. Zhang, H. Schmidt, S. Rast, M. Giorgetta, T. F. Eck, and B. Stevens (2013), MAC-v1: A new global aerosol climatology for climate studies, J. Adv. Model. Earth Syst., 5, 704–740, doi:10.1002/jame.20035.

Lacis, A., W. C. Wang, and J. Hansen, (1979), Correlated k-distribution method for radiative transfer in climate models: Application to effect of cirrus clouds on climate, NASA Conf. Publ., 2076, 309-314, 1979.

Lacis, A.A., and V. Oinas (1991), A description of the correlated k distributed method for modeling nongray gaseous absorption, thermal emission, and multiple scattering in vertically inhomogeneous atmospheres. J. Geophys. Res., 96, 9027-9063, doi:10.1029/90JD01945.

Liou, K.N. (2002), An introduction to atmospheric radiation, 2nd. Ed., Academic Press, 2002, USA.

Matthews, E. (1984), Prescription of land-surface boundary condition in GISS GCM II: A simple method based on high-resolution vegetation data bases, NASA Tech. Memo., 86096, 20 pp.

Oreopoulos, L., et al. (2012), The Continual Intercomparison of Radiation Codes: Results from Phase I, J. Geophys. Res., 117, D06118, doi:10.1029/2011JD016821.

Rossow, W. B., and A. A. Lacis (1990), Global, seasonal cloud variation from satellite radiance measurements, 2, Cloud properties and radiative effects, J. Clim., 3, 1204– 1253.

Rossow, W. B., and Y.-C. Zhang (1995), Calculation of surface and top of atmosphere radiative fluxes from physical quantities based on ISCCP data sets: 2. Validation and first results, J. Geophys. Res., 100, 1167–1197.

Rossow, W.B., Y.-C. Zhang, and J. Wang (2005), A statistical model of cloud vertical structure based on reconciling cloud layer amounts inferred from satellites and radiosonde humidity profiles. *J. Climate*, **18**, 3587-3605, doi:10.1175/JCLI3479.1.

Rothman, L.S. and coauthors, 2013, The HITRAN2012 molecular spectroscopic database, *J. Quantitative Spectroscopy & Radiative Transfer, 130(2013), 4-50.*

Schmidt, G.A. et al. (2006): Present day atmospheric simulations using GISS ModelE: Comparison to in-situ, satellite and reanalysis data. *J. Climate*, **19**, 153-192, doi:10.1175/JCLI3612.1.

Zhang, Y.-C., W. B. Rossow, and A. A. Lacis (1995), Calculation of surface and top of atmosphere radiative fluxes from physical quantities based on ISCCP data sets: 1. method and sensitivity to input data uncertainties, J. Geophys. Res., 100, 1149–1165.

Zhang, Y.-C., W.B. Rossow, A.A. Lacis, V. Oinas, and M.I. Mishchenko, 2004: Calculation of radiative fluxes from the surface to top of atmosphere based on ISCCP and other global data sets: Refinements of the radiative transfer model and the input data. *J. Geophys. Res.*, 109, D19105, doi:10.1029/2003JD004457.

Zhang, Y., W. B. Rossow, and P. W. Stackhouse Jr. (2006), Comparison of different global information sources used in surface radiative flux calculation: Radiative properties of the near-surface atmosphere, J. Geophys. Res., 111, D13106, doi:10.1029/2005JD006873.

Zhang, Y., W. B. Rossow, and P. W. Stackhouse Jr. (2007), Comparison of different global information sources used in surface radiative flux calculation: Radiative properties of the surface, J. Geophys. Res., 112, D01102, doi:10.1029/2005JD007008.

Zhang, Y., C. N. Long, W. B. Rossow, and E. G. Dutton (2010), Exploiting diurnal variations to evaluate the ISCCP-FD flux calculations and radiative-flux-analysis-processed surface observations from BSRN, ARM, and SURFRAD, J. Geophys. Res., 115, D15105, doi:10.1029/2009JD012743.

Zhang, Y.-C., W.B. Rossow, A.A. Lacis and V. Oinas (2017), the New Long-term, Global, 3-hourly, high-resolution ISCCP-FH Atmospheric Radiative Transfer Flux Profile Product, Symposium to Celebrate William B. Rossow's Science Contribution and Retirement, held in Columbia University, June 6-8, 2017.

Appendix A. Acronyms and Abbreviations

Acronym or Abbreviation	Definition
ANSI	American National Standards Institute
AOD	The aerosol optical depth
ASY	The size-related asymmetry-factor (ASY)
BSRN	The Baseline Surface Radiation Network
C-ATBD	Climate Algorithm Theoretical Basis Document
CDR	Climate Data Record
CERES	The Clouds and the Earth's Radiant Energy System (Experiment)
CF	Cloud fraction (0 – 1)
CFC	Chlorofluorocarbons
CIRC	The Continual Intercomparison of Radiation Codes
CKD	The correlated K-distribution method
CVS	Cloud vertical structure
ERBE	The Earth Radiation Budget Experiment
FOC	Full Operating Capability
GCM	The general circulation model
GEWEX	The Global Energy and Water Cycle Exchanges Project
GEWEX-SRB	The GEWEX Surface Radiation Budget
GISS	The Goddard Institute for Space Studies
H1, H2, H2X, H2Y	Intermediate dataset names for ISCCP-FH production (see Fig. 1)
HITRAN2012	The 2012 edition of the HITRAN molecular spectroscopic compilation.
IEEE	Institute of Electrical and Electronic Engineers
ICD	Interface Control Document
ifort	Int'l Composer Fortran compiler
INP	Shorten name of the INP Subproduct, the one of the 5 subproducts of ISCCP-FH
IOC	Initial Operating Capability
IR	Infrared spectrum of infrared channel of satellites
ISCCP	The International Satellite Cloud Climatology Projec
ISCCP-FH	Radiative transfer flux profile product using ISCCP H-series data products and NASA GISS RadH-PRD code.
HGG, HGH,HGM	ISCCP H-series products used for ISCCP-FH production
KD	The k-distribution method
LW	Long Wave
MACv1	The Max-Planck-Institute Aerosol Climatology version 1
MPF	Shorten name of the MPF Subproduct, the one of the 5 subproducts of ISCCP-FH, the monthly average of PRF subproduct
nnHIRS	The Neural-Network-based HIRS temperature and humidity profile dataset
NASA	The National Aeronautics and Space Administration

NASA NCCS	NASA Center for Climate Simulation
NIR	Near-infrared spectrum
NCDC	National Climatic Data Center
NOAA	National Oceanic and Atmospheric Administration
NOAA NCEI	NOAA National Centers for Environmental Information
OAD	Operational Algorithm Description
PRF	Shorten name of the PRF Subproduct, the one of the 5 subproducts of ISCCP-FH
RadD	Radiation code of NASA GISS GCM model SI2000
RadE	Radiation code of NASA GISS GCM ModelE
RadH	The radiation code recently developed based on RadE
RadH-PRD	Production code using RadH and mainly ISCCP H-series data product
RS	Reflectance
SSA	The single scattering albedo
SRF	Shorten name of the SRF Subproduct, the one of the 5 subproducts of ISCCP-FH
SW	Short Wave
Ta	Surface air temperature
Tau	Cloud optical thickness (or depth)
TC	Top temperature of cloud top
TS	Surface skin temperature
TOA	(1) Top of Atmosphere; (2) Shorten name of TOA subproduct of ISCCP-FH product
UTC	Coordinated Universal Time
UV	Ultraviolet light, electromagnetic radiation with a wavelength shorter than that of visible light but longer than X-rays (from 400 nm to 10 nm in wavelength
VCLC	Vertical cloud layer configuration
VIS	Visible spectrum or visible channel of satellites
WCRP	The world Climate Research Programme

Appendix B. Description of the extracted parameters from ISCCP-HGG product

The parameters extracted for ISCCP-FH from the original, 3-hourly ISCCP-HGG NetCDF data files are listed and briefly described in the following. All the parameters are mapped to global 110-km equal-area with 41252 cells. The serial number (in Arabic numerals) and unit are indicated for each of them under their categories; if there is no unit, unit is not shown.

I. Basic parameters (total of 12)

1. ID of broadband visible channel satellite based on the original 'satcode', -1/0/1 for undefined, non-broadband visible channel and broad band visible channel.

2. Total pixel number of a cell.

3. Surface pressure (mb).

4. Pressure at maximum temperature of the temperature profile (mb).

5. Pressure at tropopause (mb).

6. Surface air temperature (K).

7. Maximum temperature of the temperature profile (K).

8. Temperature at tropopausee (K).

9. Surface relative humidity (%).

10. Relative humidity at maximum temperature of the temperature profile (%).

11. Relative humidity at tropopause (%).

12. Column ozone amount (Dobson unit).

II. 16-level Temperature/Humidity profile (total of 32)

13 – 28. Temperature profile at 16 levels (mb).

29 – 44,. Relative humidity profile at 16 levels (%).

III. The mean properties (total of 6)

45. Mean cloud fraction (0 – 1).

46. Mean cloud top temperature (K).

47. Mean cloud optical thickness (Tau without unit).

48. Surface skin temperature (K).

49. Surface visible reflectance (0 – 1).

50. Mean Tau of the cloud water path.

III. The 18-type cloud properties (total of 72)

51 - 68. Cloud fraction of the 18 types (0-1).

69 – 86. Cloud top temperature of the 18 types (K).

87 – 104. Cloud optical thickness of the 18 types.

105 – 122. Cloud optical thickness from cloud water path.

VI. The Cloud properties from infrared (IR) channels (total of 8).

123 – 126. Mean and 3-layer cloud fraction from IR channel (0-1).

127 – 130. Mean and 3-layer cloud top temperature (K).

Appendix C. Description of the algorithm output

1. General

The ISCCP-FH production outputs 5 sub-products, namely TOA, SRF, PRF, INP and MPF subproducts as shown in the following Table. In the flux calculation, all the cloudy-sky part fluxes are based on the calculation for the 18 cloud types while clear-sky part fluxes are based on calculation under mean (clear-sky) condition. The all-sky flux is their weighted values with their relative areas within a grid cell. Their detailed definitions of parameters are given below excluding MPF's because MPF has the same contents as PRF subproduct since it is just monthly-averaged PRF.

.

Subproduct Abbrev. Name	Definition	Total number of parameters
TOA	Top-of-Atmosphere Radiative Fluxes with summary inputs	23
SRF	Surface Radiative Fluxes with summary inputs	34
PRF	5-level Profile Fluxes for surface, 680, 440 & 100 mb and TOA with summary inputs	91
INP	Comprehensive input variables for ISCCP-FH production	Up to 335
MPF	Monthly average of PRF	91

2. List of TOA Sub-product parameters

(A) Original

(1) Surface pressure (mb);
(2) Surface skin temperature (K);
(3) Surface SW (0.2-5.0 μm) albedo (0-1) without atmosphere;
(4) Surface LW (5.0-200 μm) emissivity (0-1) without atmosphere;
(5) Total column precipitable water for all sky (cm);
(6) Cosine solar zenith angle (0-1);
(7) Total column ozone (Dobson units);
(8) Temperature at 500 mb (K);
(9) Precipitable water of 560-440 mb layer for all sky (cm);
(10) Mean cloud fraction (0-1);
(11) Total column cloud optical thickness;
(12) Pressure of topmost level of cloud layer(s) (mb);
(13) Pressure of lowest base of cloud layer(s) (mb);

(14) Temperature of topmost level of cloud layer(s) (K);
(15) Temperature of lowest base of cloud layer(s) (K);
(16) Total column AOD of 0.55 μm;
(17) SW downwelling at TOA (W/m^2);
(18) SW upwelling for all sky at TOA (W/m^2);
(19) LW upwelling for all sky at TOA (W/m^2);
(20) SW upwelling for clear sky at TOA (W/m^2);
(21) LW upwelling for clear sky at TOA (W/m^2);

(B) Derived from above when using TOA subproduct

(22) SW upwelling for 100% overcast sky at TOA (W/m^2);
(23) LW upwelling for 100% overcast sky at TOA (W/m^2);

3. List of SRF Sub-product parameters

(A) Original

(1) Surface pressure (mb);
(2) Surface skin temperature (K);
(3) Surface SW (0.2-5.0 μm) albedo (0-1) without atmosphere;
(4) Surface LW (5.0-200 μm) emissivity (0-1) without atmosphere;
(5) Total column precipitable water for all sky (cm);
(6) Cosine solar zenith angle (0-1);
(7) Total column ozone (Dobson units);
(8) Surface air temperature (K);
(9) Precipitable water for 200-mb-thick layer sitting on the surface for all sky (cm);
(10) Mean cloud fraction (0-1);
(11) Total column cloud optical thickness;
(12) Pressure of topmost level of cloud layer(s) (mb);
(13) Pressure of lowest base of cloud layer(s) (mb);
(14) Temperature of topmost level of cloud layer(s) (K);
(15) Temperature of lowest base of cloud layer(s) (K);
(16) Total column AOD of 0.55 μm;
(17) SW-direct downwelling for all sky at surface (W/m^2);
(18) SW-diffuse downwelling for all sky at surface (W/m^2);

(19) SW downwelling for all sky at surface (W/m^2);
(20) SW upwelling for all sky at surface (W/m^2);
(21) LW downwelling for all sky at surface (W/m^2);
(22) LW upwelling for all sky at surface (W/m^2);
(23) SW-direct downwelling for clear sky at surface (W/m^2);
(24) SW-diffuse downwelling for clear sky at surface (W/m^2);
(25) SW downwelling for clear sky at surface (W/m^2);
(26) SW upwelling for clear sky at surface (W/m^2);
(27) LW downwelling for clear sky at surface (W/m^2);
(28) LW upwelling for clear sky at surface (W/m^2);

(B) Derived from above when using SRF subproduct

(29) SW-direct downwelling for 100% overcast sky at surface (W/m^2);
(30) SW-diffuse downwelling for 100% overcast sky at surface (W/m^2);
(31) SW downwelling for 100% overcast sky at surface (W/m^2);
(32) SW upwelling for 100% overcast sky at surface (W/m^2);
(33) LW downwelling for 100% overcast sky at surface (W/m^2);
(34) LW upwelling for 100% overcast sky at surface (W/m^2);

4. List of PRF Sub-product parameters

(A) Original

(1) Surface pressure (mb);
(2) Surface skin temperature (K);
(3) Surface SW (0.2-5.0 μm) albedo (0-1) without atmosphere;
(4) Surface LW (5.0-200 μm) emissivity (0-1) without atmosphere;
(5) Total column precipitable water for all sky (cm);
(6) Cosine solar zenith angle (0-1);
(7) Total column ozone (Dobson units);
(8) Surface air temperature (K);
(9) Temperature at 500 mb (K);
(10) Precipitable water for 200-mb-thick layer sitting on the surface for all sky (cm) ;
(11) Precipitable water of 560-440 mb layer for all sky (cm);

(12) Total column AOD of 0.55 μm;
(13) Type 1 cloud fraction (0-1) for type-cloud calculation;
(14) Type 2 cloud fraction (0-1) for type-cloud calculation;
(15) Type 3 cloud fraction (0-1) for type-cloud calculation;
(16) Type 4 cloud fraction (0-1) for type-cloud calculation;
(17) Type 5 cloud fraction (0-1) for type-cloud calculation;
(18) Type 6 cloud fraction (0-1) for type-cloud calculation;
(19) Type 7 cloud fraction (0-1) for type-cloud calculation;
(20) Type 8 cloud fraction (0-1) for type-cloud calculation;
(21) Type 9 cloud fraction (0-1) for type-cloud calculation;
(22) Type 10 cloud fraction (0-1) for type-cloud calculation;
(23) Type 11 cloud fraction (0-1) for type-cloud calculation;
(24) Type 12 cloud fraction (0-1) for type-cloud calculation;
(25) Type 13 cloud fraction (0-1) for type-cloud calculation;
(26) Type 14 cloud fraction (0-1) for type-cloud calculation;
(27) Type 15 cloud fraction (0-1) for type-cloud calculation;
(28) Type 16 cloud fraction (0-1) for type-cloud calculation;
(29) Type 17 cloud fraction (0-1) for type-cloud calculation;
(30) Type 18 cloud fraction (0-1) for type-cloud calculation;
(31) SW-direct downwelling for all sky at surface (W/m^2);
(32) SW-diffuse downwelling for all sky at surface (W/m^2);
(33) SW-direct downwelling for clear sky at surface (W/m^2);
(34) SW-diffuse downwelling for clear sky at surface (W/m^2);
(35) SW downwelling for all sky at surface (W/m^2);
(36) SW upwelling for all sky at surface (W/m^2);
(37) LW downwelling for all sky at surface (W/m^2);
(38) LW upwelling for all sky at surface (W/m^2);
(39) SW downwelling for all sky at 680 mb (W/m^2);
(40) SW upwelling for all sky at 680 mb (W/m^2);
(41) LW downwelling for all sky at 680 mb (W/m^2);
(42) LW upwelling for all sky at 680 mb (W/m^2);
(43) SW downwelling for all sky at 440 mb (W/m^2);
(44) SW upwelling for all sky at 440 mb (W/m^2);
(45) LW downwelling for all sky at 440 mb (W/m^2);
(46) LW upwelling for all sky at 440 mb (W/m^2);
(47) SW downwelling for all sky at 100 mb (W/m^2);
(48) SW upwelling for all sky at 100 mb (W/m^2);

(49) LW downwelling for all sky at 100 mb (W/m^2);
(50) LW upwelling for all sky at 100 mb (W/m^2);
(51) SW downwelling at TOA (W/m^2);
(52) SW upwelling for all sky at TOA (W/m^2);
(53) LW upwelling for all sky at TOA (W/m^2);
(54) SW downwelling for clear sky at surface (W/m^2);
(55) SW upwelling for clear sky at surface (W/m^2);
(56) LW downwelling for clear sky at surface (W/m^2);
(57) LW upwelling for clear sky at surface (W/m^2);
(58) SW downwelling for clear sky at 680 mb (W/m^2);
(59) SW upwelling for clear sky at 680 mb (W/m^2);
(60) LW downwelling for clear sky at 680 mb (W/m^2);
(61) LW upwelling for clear sky at 680 mb (W/m^2);
(62) SW downwelling for clear sky at 440 mb (W/m^2);
(63) SW upwelling for clear sky at 440 mb (W/m^2);
(64) LW downwelling for clear sky at 440 mb (W/m^2);
(65) LW upwelling for clear sky at 440 mb (W/m^2);
(66) SW downwelling for clear sky at 100 mb (W/m^2);
(67) SW upwelling for clear sky at 100 mb (W/m^2);
(68 LW downwelling for clear sky at 100 mb (W/m^2);
(69) LW upwelling for clear sky at 100 mb (W/m^2);
(70) SW upwelling for clear sky at TOA (W/m^2);
(71) LW upwelling for clear sky at TOA (W/m^2);

(B) Derived from above when using PRF subproduct

(72) SW-direct downward for 100% overcast sky at surface (W/m^2);
(73) SW-diffuse downward for 100% overcast sky at surface (W/m^2);
(74) SW downwelling for 100% overcast sky at surface (W/m^2);
(75) SW upwelling for 100% overcast sky at surface (W/m^2);
(76) LW downwelling for 100% overcast sky at surface (W/m^2);
(77) LW upwelling for 100% overcast sky at surface (W/m^2);
(78) SW downwelling for 100% overcast sky at 680 mb (W/m^2);
(79) SW upwelling for 100% overcast sky at 680 mb (W/m^2);
(80) LW downwelling for 100% overcast sky at 680 mb (W/m^2);
(81) LW upwelling for 100% overcast sky at 680 mb (W/m^2);
(82) SW downwelling for 100% overcast sky at 440 mb (W/m^2);

(83) SW upwelling for 100% overcast sky at 440 mb (W/m^2);
(84) LW downwelling for 100% overcast sky at 440 mb (W/m^2);
(85) LW upwelling for 100% overcast sky at 440 mb (W/m^2);
(86) SW downwelling for 100% overcast sky at 100 mb (W/m^2);
(87) SW upwelling for 100% overcast sky at 100 mb (W/m^2);
(88 LW downwelling for 100% overcast sky at 100 mb (W/m^2);
(89) LW upwelling for 100% overcast sky at 100 mb (W/m^2);
(90) SW upwelling for 100% overcast sky at TOA (W/m^2);
(91) LW upwelling for 100% overcast sky at TOA (W/m^2);

5. List of INP Sub-product parameters

(1) Surface pressure (mb);
(2) Surface skin temperature (K);
(3) Surface SW (0.2-5.0 μm) albedo (0-1) without atmosphere;
(4) Surface LW (5.0-200 μm) emissivity (0-1) without atmosphere;
(5) Cosine solar zenith angle (0-1);
(6) Total column ozone (Dobson units);
(7) Surface air temperature (K);
(8) Temperature at 900 mb (K);
(9) Temperature at 740 mb (K);
(10) Temperature at 620 mb (K);
(11) Temperature at 500 mb (K);
(12) Temperature at 375 mb (K);
(13) Temperature at 245 mb (K);
(14) Temperature at 125 mb (K);
(15) Temperature at 50 mb (K);
(16) Temperature at 15 mb (K);
(17) Precipitable water of 1000-800 mb layer for all sky (cm);
(18) Precipitable water of 800-680 mb layer for all sky (cm);
(19) Precipitable water of 680-560 mb layer for all sky (cm);
(20) Precipitable water of 560-440 mb layer for all sky (cm);
(21) Precipitable water of 440-310 mb layer for all sky (cm);
(22) Precipitable water of 310-180 mb layer for all sky (cm);
(23) Precipitable water of 180- 70 mb layer for all sky (cm);
(24) Precipitable water of 70- 30 mb layer for all sky (cm);
(25) Precipitable water of 30- 0 mb layer for all sky (cm);
(26) Tropospheric total column AOD of 0.55 μm;

(27) Stratospheric (volcanic) total column AOD of 0.55 μm;
(28) Dusts' total column AOD of 0.55 μm;
(29) Number of total existent cloud types (of a cell);
(30) Type 1 cloud fraction (0-1) for type-cloud calculation;
(31) Type 2 cloud fraction (0-1) for type-cloud calculation;
(32) Type 3 cloud fraction (0-1) for type-cloud calculation;
(33) Type 4 cloud fraction (0-1) for type-cloud calculation;
(34) Type 5 cloud fraction (0-1) for type-cloud calculation;
(35) Type 6 cloud fraction (0-1) for type-cloud calculation;
(36) Type 7 cloud fraction (0-1) for type-cloud calculation;
(37) Type 8 cloud fraction (0-1) for type-cloud calculation;
(38) Type 9 cloud fraction (0-1) for type-cloud calculation;
(39) Type 10 cloud fraction (0-1) for type-cloud calculation;
(40) Type 11 cloud fraction (0-1) for type-cloud calculation;
(41) Type 12 cloud fraction (0-1) for type-cloud calculation;
(42) Type 13 cloud fraction (0-1) for type-cloud calculation;
(43) Type 14 cloud fraction (0-1) for type-cloud calculation;
(44) Type 15 cloud fraction (0-1) for type-cloud calculation;
(45) Type 16 cloud fraction (0-1) for type-cloud calculation;
(46) Type 17 cloud fraction (0-1) for type-cloud calculation;
(47) Type 18 cloud fraction (0-1) for type-cloud calculation;
(48) Number of cloud layers for above type 1;
(49) Number of cloud layers for above type 2;
(50) Number of cloud layers for above type 3;
(51) Number of cloud layers for above type 4;
(52) Number of cloud layers for above type 5;
(53) Number of cloud layers for above type 6;
(54) Number of cloud layers for above type 7;
(55) Number of cloud layers for above type 8;
(56) Number of cloud layers for above type 9;
(57) Number of cloud layers for above type 10;
(58) Number of cloud layers for above type 11;
(59) Number of cloud layers for above type 12;
(60) Number of cloud layers for above type 13;
(61) Number of cloud layers for above type 14;
(62) Number of cloud layers for above type 15;
(63) Number of cloud layers for above type 16;

(64) Number of cloud layers for above type 17;
(65) Number of cloud layers for above type 18;

(66) – (155): Optical thickness for up to 5 cloud layer of 18 cloud types (cloud layers are counted from surface to TOA);
(156) – (245): Cloud top pressure for up to 5 cloud layer of 18 cloud types;
(246) – (335): Cloud base pressure for up to 5 cloud layer of 18 cloud types ;